ELSEVIER

Magnetic Resonance Imaging 21 (2003) 651–661

MAGNETIC RESONANCE IMAGING

Computational modeling of cerebral diffusion-application to stroke imaging

K. Khanafer[a], K. Vafai[a,*], A. Kangarlu[b]

[a]*Department of Mechanical Engineering, University of California, Riverside, CA 92521 USA*
[b]*Center for Advanced Biomedical Imaging, Department of Radiology, The Ohio State University, Columbus, OH 43210 USA*

Received 9 January 2002; accepted 20 February 2003

Abstract

Water diffusion within the structure of a brain extracellular space is analyzed numerically for various diffusion parameters of brain tissue namely extracellular space porosity and tortuosity. An algorithm for predicting diffusion pattern of water molecules within human brain considering the mechanics of water diffusion within porous media is developed. The extracellular space is modeled as a homogeneous porous medium with uniform porosity and permeability. Discretization of the fluid flow, heat transfer and mass transport equations is achieved using a finite element scheme based on the Galerkin method of weighted residuals. Concentration maps are developed in this study for various clinical conditions. The effect of the space porosity and the turtousity on the heat and mass transport within the extracellular space are found to be significant. The results presented in this work play an important role in producing more effective imaging techniques for brain injury based on the apparent diffusion coefficient.

Keywords: Apparent diffusion coefficient; Diffusion-weighted MR imaging; Porous; Stroke

1. Introduction

Magnetic resonance imaging (MRI) is a powerful technique for the *in vivo* measurement of the diffusion of water and intracellular metabolites. Recently diffusion-weighted magnetic resonance imaging (DW-MRI) has become valuable research and clinical imaging modality for the noninvasive detection and characterization of cerebral ischemia. Diffusion-weighted imaging, which is based on the molecular diffusion coefficient in vivo, is sensitive to cerebral ischemia within minutes of the onset of stroke. This technique shows superior capabilities in the early prediction of the brain stroke compared to the conventional imaging techniques such as T_1-, T_2-weighted magnetic resonance imaging and CT for patients not receiving any treatment [1]. Moreover, DW-MRI technique provides significant information about the structure and the spatial organization of the brain tissue compartments and about the water exchange between these compartments in normal and diseased states [2]. Strong magnetic field gradient pulses are incorporated into an imaging pulse sequence to obtain the images. In a diffusion-weighted image, areas with fast diffusion are dark because they are subject to greater signal attenuation, while bright areas are associated with slow diffusion process.

To increase our understanding of the cellular response to pathologic conditions especially the prediction of the acute ischemic stroke, the apparent diffusion coefficient (ADC) is determined in the brain tissue. This term is used to quantitatively analyze the results of diffusion in vivo and accordingly helps in the early diagnosis of stroke, assessment of white matter diseases and monitoring of tissue temperature change during hyperthermia or laser surgery. It has been reported in the literature that several minutes after the onset of the stroke, there is a significant drop in the apparent diffusion coefficient.

The significant changes in the apparent diffusion coefficient (ADC) of water that occur in ischemic brain are of considerable importance. Several studies have been conducted in the literature to better understand the mechanisms that account for the changes seen in the ischemia. The leading hypothesis suggests that cellular swelling associated with the failure of the ionic gradient across the cell membrane results in an increase in extracellular (ECS) tortuosity of the diffusion paths. Others suggest that the influx of

* Corresponding author. Tel.: +1-909-787-2135; fax: +1-909-787-2899.
E-mail address: vafai@engr.ucr.edu (K. Vafai).

0730-725X/03/$ – see front matter
doi:10.1016/S0730-725X(03)00091-2

Nomenclature

D	Diffusion coefficient
e_r, e_ϕ	unit vectors in the radial, and angular directions, respectively
$\vec{g}$	gravitational acceleration vector
Gr_C	solutal Grashof number, $g\,\beta_C \Delta C' r_o^3/\nu^2$
Gr_T	Grashof number, $g\beta_T \Delta T r_o^3/\nu^2$
k	thermal conductivity
Le	Lewis number, α/D
N	buoyancy ratio, $\beta_C \Delta C'/\beta_T \Delta T = Gr_c/Gr_T$
P	dimensionless pressure
Pr	Prandtl number, ν/α
r_i	inner cylinder radius
r_o	outer cylinder radius
R	radii ratio, r_o/r_i
Sc	Schmidt number, ν/D
t	time
T	temperature
u, v	nondimensional velocity components in the radial, and angular directions, respectively.
u	velocity vector
x, y	Cartesian coordinates
X, Y	dimensionless coordinates.

Greek Symbols

α	thermal diffusivity
β_T	thermal expansion coefficient
β_C	solutal expansion coefficient
ρ_o	density at reference temperature
κ	permeability
ε	porosity
ϕ	angular coordinate
ψ	stream function
θ	dimensionless temperature, $(T - T_o)/(T_i - T_o)$
ν	kinematic viscosity

Subscripts

i	inner cylinder
o	outer cylinder

fast-diffusing extracellular water, that occurs during cellular swelling, increases the proportion of water in the intracellular space (ICS), which is more restricted and viscous than the extracellular space (ECS). Norris et al. [3] and Latour et al. [4] concluded that the ADC drop in stroke is due to an increase in the tortuosity of the available pathways for fast diffusion within the extracellular space. Moseley et al. [5], Mintorovitch et al. [6] and Benveniste et al. [7] referred the reduction in the ADC to the cell swelling which causes water molecules to move from extracellular space to the intracellular space, where the diffusion process may be slower, so the overall ADC drops. Helpern et al. [8] have suggested that the reduction in the cell membrane permeability causes a significant decrease in the apparent diffusion coefficient (ADC) after acute injury.

Moseley et al. [9] demonstrated for the first time that diffusion-weighted imaging (DWI) could detect ischemic stroke within minutes of vascular occlusion. Since then DWI has become an integral part of the evaluation of ischemic stroke particularly under acute conditions. CT and conventional MR sequences are insensitive to early ischemic changes whereas DWI has been shown to be positive within as early as 30 min in humans. DWI is ideal for the evaluation of patients with acute ischemic stroke because of its high sensitivity and specificity, and very short imaging times which make it highly resistant to patient motion, a common problem with imaging stroke patients. However, diffusion imaging is not perfect. Although an early drop in diffusion was initially thought to represent a marker of inevitable and irreversible neuronal death, reported cases of reversibility of diffusion abnormalities indicate that diffusion abnormalities represent ischemic injury that may be reversible. The challenge is to develop DWI into a quantitative method for measuring ischemic injury, which could serve as the basis for intervention, therapy and prediction of outcome.

The signal changes seen with DWI appear to be the result of cytotoxic edema. Occlusions of cerebral vessels lead to a decrease in cerebral blood flow, which results in disruption of energy metabolism. Disruption of the Na/K ATP pump leads to loss of ionic gradients and a net influx of water from the extracellular space to the intracellular compartment where mobility of water is restricted. This leads to the signal changes on DWI and ADC imaging. As soon as the circulation is re-established assuming the tissue is viable, energy metabolism begins to recover, the ion pumps are reactivated and water and ion equilibration occurs. Reversal of ischemic injury results in reversal of diffusion abnormalities. It has been suggested that it is possible to establish a direct relationship between the diffusion properties and the metabolic state of tissue using ADC imaging. Back et al. [10] showed that the reduction of the ADC reflects the region of histologic injury, breakdown of energy metabolism and tissue acidosis. If this can be done in vivo, this could allow for possible quantification of ischemia and determination of viable tissue versus irreparably damaged brain tissue thus determining which patients would benefit from treatment and which may be harmed.

The development of high field (HF) MRI has ushered in an opportunity for high sensitivity events to be monitored. The advantages of HFMRI such as signal to noise will help to bring insight into the physiologic basis of diffusion imaging. For example, the nature of the diffusion process and its multiexponential behavior could better be discovered at high field. Diffusion images acquired at high field would also be able to account for mechanisms such as extracellular porosity (ECS) induced contrast. Such images will more accurately represent the examined tissues. Once ECS is accounted for an in-vivo DWI, its capability for clinical

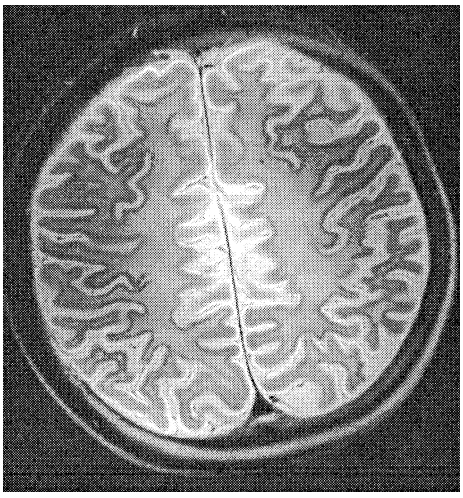

Fig. 1. A human cadaver head image acquired at 8 Tesla in axial direction just superior to the lateral ventriclesA stimulated echo diffusion weighted (STE-DWI) sequence with the following parameters were used TR = 1000 ms, TE = 75 msec, δ = 5-30 mT/m, Δ = 40 ms, FOV = 20 cm, slice thickness = 2 mm.

diagnosis will be greatly enhanced. We propose diffusion studies at high field in order to incorporate ECS clinically relevant to DWI images. Our initial results are promising in the sense that DWI weighted images possess contrast that has not previously been observed at lower fields, see Fig. 1. In this Figure, an axial image of a human cadaver taken at 8 Tesla is shown. This image was acquired using stimulated echo (STE) with pulsed field gradients with diffusion gradient strength producing b values up to $b = 1000$ s/mm^2. Such diffusion sequence, however, will not be practical for in-vivo human applications because of long acquisition times and motion. Nevertheless, the valuable information that HF DWI contains calls for a further examination of diffusion technique and modification of diffusion-based pulse sequences. A closer look at Fig. 1 shows high signal intensity from the cerebral spinal fluid (CSF) spaces. Also, the white matter/gray matter is well differentiated. In addition, the gray/white boundary is exquisitely visualized. This may be due to the structural differences such as density and porosity pattern in gray matter leading to greater signal loss. The image has a resolution of 390 micron in-plane which is much higher (10 to 20 times) than the routine DWI images acquired at 1.5T. This image indicates that HF DWI could emerge as a useful imaging method for non-invasive evaluation of the motion of water at the molecular level in the brain. Through HF DWI, it is possible to more accurately measure diffusivity, which is a measure of the magnitude of the diffusion. Increased diffusivity is observed as a result of a change in the microstructural environment secondary to the tissue pathology.

In the neuroscience context, the extracellular space (ECS) constitutes the microenvironment of brain cells. It is a conduit for cellular metabolities, a channel for chemical signaling mediated by volume transmission, and a route for drug delivery [11]. Therefore, the extracellular space represents a significant communication channel between neurons, and between neurons and glial cells [12,13,14]. From a physical perspective, the extracellular space of the brain resembles that of a porous medium. The diffusion process within the extracellular space affects the activity level of the substances in the ECS and their movement toward the adjacent neurons and glial cells and the access of neurohormones released from axons to the capillaries [15]. Any change in the parameters that influence the diffusion process within the ECS can substantially affect the intercellual signal transmission. Such parameters include the porosity of the ECS (the void volume of the tissue which is available for diffusion of substances) and the ECS tortuosity. Nicholson and Phillips [16] conducted a study on the diffusion in the brain-cell microenvironment using the simple diffusion equation in a simple medium with an effective diffusion coefficient and with an altered source term. Dai and Miura [17] built a lattice cellular automate model for ion diffusion within the brain-cell microenvironment and performed numerical simulations using the corresponding lattice Boltzmann equation. The effects of the tortuosity and the volume fraction on the movement of ions by diffusion is analyzed.

Recently, Khanafer et al. [18] studied numerically water diffusion within the brain in the absence of porous medium for a wide range of pertinent parameters such as Lewis number, cell volume, and the buoyancy ratio. The results show that the diffusion coefficient, cell volume, and the buoyancy ratio play significant roles on the characterization of the mass and heat transfer mechanisms within the cell. The objective of the present study is to obtain a detailed understanding of the factors that affect ADC of water in brain tissues. The extracellular milieu of a neurone contains ions, metabolic substrates and neuroactive compounds that change dynamically during neural activity and can significantly influence the transmission of information in the nervous tissue. Diffusion process is a crucial factor in the distribution of the extracellular substrates and accordingly the determination of the effects of the porosity and the tortuosity on the diffusion process within the brain structure is one of the objectives of this research. In this work we propose an algorithm for predicting diffusion pattern of water molecules within human brain considering the mechanics of water diffusion within porous media. Modeling will use simple structures as well as structures with complexities comparable to human brain. The model will evaluate the major challenges in applying such a tool to pathology, in particular stroke. Solutions to current challenges in modeling diffusion for human cerebral tissue for the purpose of developing a technique sensitive to tissue viability after ischemic stroke will be proposed.

The model will ultimately lead into a new MRI technique

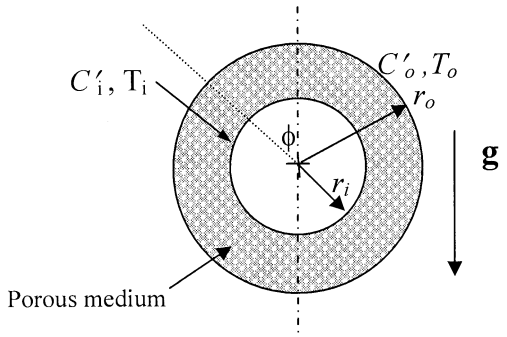

Fig. 2. Schematic of the physical model and coordinate system.

with the ability to identify the "death domain" for brain cells. This condition, in which a cascade of molecular events is initiated causing a process of self-destruction by the cell, has never been visualized in human or animals before. In fact, by specific modeling of the diffusion mechanism and peculiarities in porous media and ability to translate these effects into imaging contrast we could develop a technique for visualization of apoptosis.

2. Mathematical formulation

Consider a tissue model in which the brain is represented by two horizontal concentric cylinders filled with a fluid-saturated porous medium. The geometry of the problem and the coordinate system are shown in Fig. 2. The porous medium of porosity ε and permeability κ is saturated with an incompressible Newtonian fluid. Variable porosity model is incorporated in this investigation to illustrate its effects on the tissue's apparent diffusion coefficient (see for instance, Vafai [19,20]). The fluid contained within the cell is assumed to be laminar. The inner cylinder of radius r_i is kept at a higher temperature and concentration (T_i and C_i') while the outer cylinder of radius r_o is kept at lower temperature and concentration T_o and C_o').

The variation in the thermophysical properties of the fluid is considered in this investigation. The density variation in the buoyancy force is approximated according to the Boussinesq approximation. This variation, due to both temperature and concentration gradients, can be described by the following equation:

$$\rho = \rho_o[1 - \beta_T (T - T_o) - \beta_C (C' - C_o')] \tag{1}$$

where β_T and β_C are the coefficients for thermal and concentration expansions, respectively:

$$\beta_T = -\frac{1}{\rho_o}\left(\frac{\partial \rho}{\partial T}\right)_{P,C} \beta_C = -\frac{1}{\rho_o}\left(\frac{\partial \rho}{\partial C'}\right)_{P,T} \tag{2}$$

To render the equations nondimensional, the following dimensionless parameters are used:

$$R_i = \frac{r_i}{r_o}, R_o = \frac{r_o}{r_o} = 1, \mathbf{u} = \frac{(u,v)r_o}{\alpha\sqrt{RaPr}}, \tau = \frac{ta\sqrt{Ra\ Pr}}{r_o^2}$$

$$\theta = \frac{T - T_o}{T_i - T_o}, C = \frac{C' - C_o'}{C_i' - C_o'}, P = \frac{pr_o^2}{\mu\alpha\sqrt{Ra\ Pr}} \tag{3}$$

The mathematical formulation for the present investigation taking into account the above mentioned assumptions is written in nondimensional form based on the analysis presented by Vafai and Tien [21] as follows:

$$\nabla \cdot \mathbf{u} = 0 \tag{4}$$

$$\frac{\partial \mathbf{u}}{\partial t} = -\nabla P + \frac{\nabla^2 \mathbf{u}}{\sqrt{Gr}} - \frac{\varepsilon \mathbf{u}}{Da\sqrt{Gr_T}} - \frac{\varepsilon^2 F}{\sqrt{Da}}|\mathbf{u}|\mathbf{u} + \mathbf{g}([\theta + NC]\cos\phi e_r - [\theta + NC]\sin\phi e_\phi) \tag{5}$$

$$\left(\frac{\partial T}{\partial t} + (\mathbf{u}\cdot\nabla)T\right) = \frac{\nabla^2\theta}{Pr\sqrt{Gr_T}} \tag{6}$$

$$\left(\frac{\partial C}{\partial t} + (\mathbf{u}\cdot\nabla)C\right) = \frac{\nabla^2 C}{Sc\sqrt{Gr_T}} \tag{7}$$

where $\mathbf{u}$ is the velocity vector (u, v) and N is buoyancy ratio, $N = \beta_C\Delta C'/\beta_T\Delta T = Gr_C/Gr_T$, The nondimensional parameters in the above equations are Darcy number Da, $Da = \kappa/r_o^2$, Grashof number Gr_T, $Gr_T = g\beta_T(T_i - T_o)r_o^3/\nu^2$, Prantl number Pr, $Pr = \nu/\alpha$, and Schmidt number Sc, $Sc = \nu/D$, respectively. In these equations κ, ν, D, and α are the permeability of the porous medium, kinematic viscosity, diffusion coefficient, and the thermal diffusivity of the fluid, respectively. β_T and β_c are the thermal expansion and the solutal expansion coefficients, respectively. F is a function that depends on the Reynolds number and the microstructure of the porous medium [21] and ϵ is the porosity. It should be noted that the convective terms in the generalized momentum equation, Eq. (5), are dropped based on the analysis given by Vafai and Tien [21].

The medium permeability κ and the geometric function F are given in (Vafai [19], Vafai [20], Amiri and Vafai [22], and Amiri et al. [23])

$$\kappa = \frac{\varepsilon^3 d_p^2}{150(1-\varepsilon)^2}, F = \frac{1.75}{\sqrt{150\varepsilon^3}} \tag{8}$$

The initial conditions for the present investigation are given by

$$u = v = \theta = C = 0 \qquad \text{at } t = 0 \tag{9}$$

The boundary conditions for the problem under consideration are expressed as:

$$u = v = 0,\ C = \theta = 1 \qquad \text{at } R_i = \frac{r_i}{r_o} \tag{10}$$

$$u = 0,\ v = 0,\ C = \theta = 0 \qquad \text{at } R_o = 1 \tag{11}$$

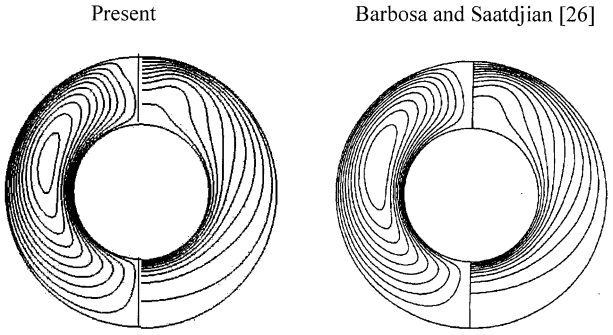

Fig. 3. Comparison of the streamlines and isotherms between the present solution and that of Barbosa and Saatdjian [26] in a porous horizontal cylindrical annulus ($Ra = 100$, $R_o/R_i = 2$).

3. Numerical method

A finite element formulation based on the Galerkin method will be employed to solve the governing equations subject to the initial and boundary conditions for the present study. The application of this technique is well described by Taylor and Hood [24] and Gresho et al. [25] and its application is well documented [26]. The highly coupled and non-linear algebraic equations resulting from the discretization of the governing equations are solved using an iterative solution scheme using the segregated solution algorithm. The advantage of using this method is that the global system matrix is decomposed into smaller submatrices and then solved in a sequential manner. This technique will result in considerably fewer storage requirements. The conjugate residual scheme is used to solve the symmetric pressure-type equation systems, while the conjugate gradient squared is used for the non-symmetric advection-diffusion-type equations. A variable grid-size system is implemented in the present investigation especially near the walls to capture the rapid changes in the dependent variables. Extensive numerical experimentation is also performed to attain grid-independent results for all the field variables. When the relative change in variables between consecutive iterations is less than 10^{-6}, convergence is assumed to have been achieved.

The validation of the present numerical code is performed against the work of Barbosa and Saatdjian [27] in a porous horizontal cylindrical annulus for a radius ratio of 2 and a Rayleigh number of 100 as shown in Fig. 3. The comparison shows excellent agreement between the present result and other works available in the literature. Moreover, the validation of the numerical code was performed against the work of Weaver and Viskanta [27] in the absence of porous medium as shown in Fig. 4. It can be seen from this Figure that the solution of the present numerical code is in excellent agreement with the numerical and experimental results of Weaver and Viskanta [28] for Grashof numbers of $Gr_T = 5.88 \times 10^5$, 9.31×10^5 and buoyancy ratios of $N = 0.55, -1.85$.

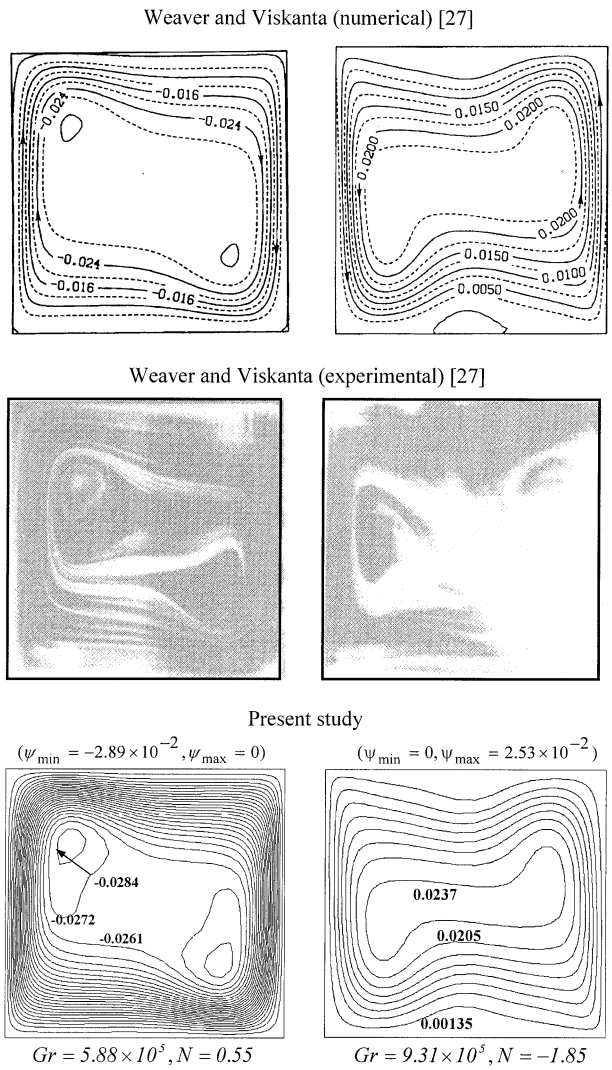

Fig. 4. Comparison of the streamlines between the present numerical solution and that of Weaver and Viskanta [27].

4. Discussion and results

Diffusion process within the extracellular space is simulated numerically in the present investigation for various pertinent parameters. These parameters include the effect of the extracellular space porosity and turtousity, permeability of the porous medium (Darcy number), Lewis number, Buoyancy ratio, and Grashof number.

The effect of the porosity of the extracellular space on the isoconcentrations, streamlines, and isotherms contours is shown in Fig. 5. Porosity is defined as the ratio of the void volume to the total volume of the extracellular space. As the porosity increases, the void volume increases and accordingly more open space is available for the fluid to move in the extracellular space. Moreover, it is clear that for higher porosity, the resistance forces created by the porous medium are less significant leading to higher dimensionless velocities as illustrated by higher fluid circulations. For lower

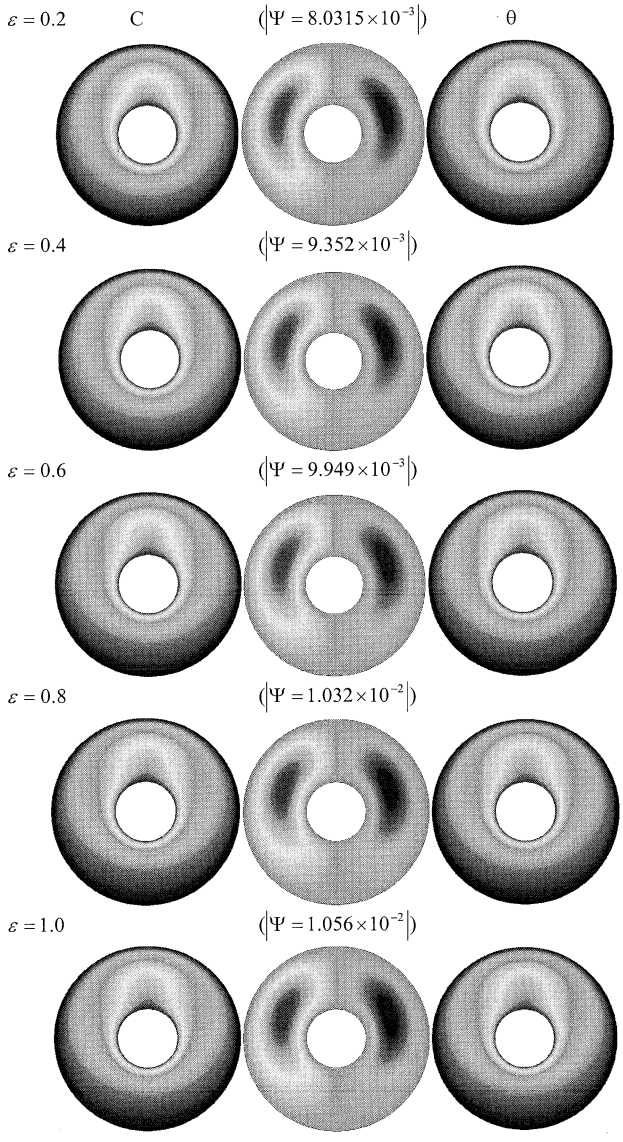

Fig. 5. The effect of the porosity on the isoconcentrations, streamlines, and the isotherms ($Da = 10^{-3}$, $Gr = 10^4$, $Le = 1.0$, $N = 1.0$).

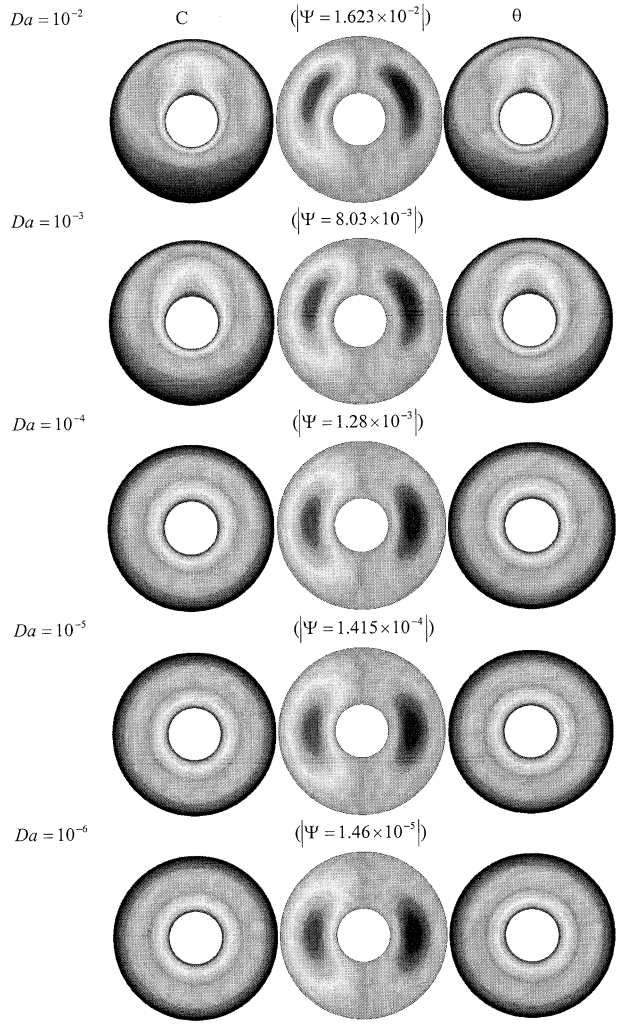

Fig. 6. Effect of the Darcy number on the isoconcentrations, streamlines, and the isotherms ($Gr = 10^4$, $Le = 1.0$, $N = 1.0$, $\varepsilon = 0.2$).

values of porosity, Fig. 5 shows that the diffusion process is slow in the extracellular space.

The effect of the Darcy number on the isoconcentrations, streamlines and the isotherms is illustrated in Fig. 6. Darcy number measures the permeability of the porous medium and accordingly the resistance to the flow velocity through ECS. For large Darcy number ($Da = 10^{-2}$), the permeability of the medium is large which results in higher heat and mass transfer rates within ECS as depicted in Fig. 6. However, as the Darcy number decreases, the convective heat transfer process suppresses within the ECS as well as the mass transfer of the substance and this is associated with a lower permeability. In addition, it can be seen from this figure that as the Darcy number decreases, the isoconcentration and the isotherm patterns change significantly resulting in a pure diffusion regime. In this case, isoconcentrations and isotherms resemble concentric circles for small Darcy numbers. This is due to the bulk damping caused by the presence of the porous matrix. Fig. 6 illustrates that the circulation of the fluid within the ECS substantially reduces as the Darcy number decreases.

The effect of the Darcy number on the velocity components of the fluid within the extracellular space is depicted in Fig. 7. It is clearly seen in this figure that the velocities within the ECS are substantially decreased as the Darcy number decreases. For small values of the Darcy number ($Da = 10^{-6}$), the fluid experiences a pronounced large resistance as it flows through the porous matrix causing the flow to cease in the bulk of the cavity. In this situation, the convective heat transfer mechanism is completely suppressed as well as the thermosolutal activities indicating pure heat and mass diffusion regimes in the ECS.

The influence of the thermal Grashof number on the isoconcentrations, streamlines and the isotherms is

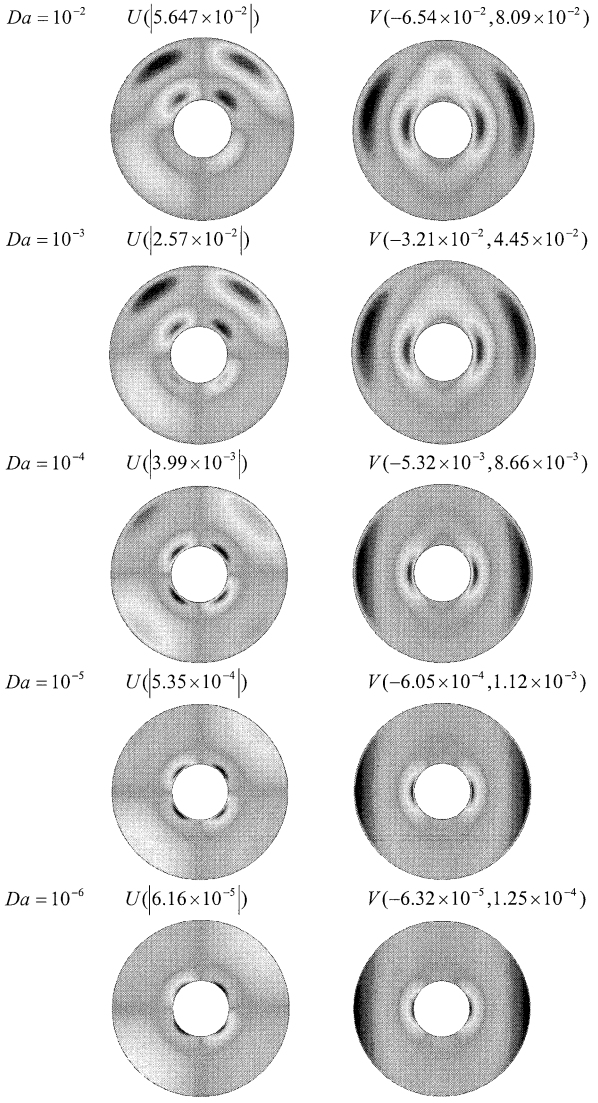

Fig. 7. Effect of the Darcy number on the velocity components ($Gr = 10^4$, $Le = 1.0$, $N = 1.0$, $\varepsilon = 0.2$).

shown in Fig. 8. It is well known that the Grashof number characterizes the influence of the external forces on the convective motion within the extracellular space. For a Grashof number of $10^{3,}$ Fig. 8 indicates that the heat transfer and the mass transfer processes within the space is mainly by diffusion. As the Grashof number increases, the intensity of convection motion as well as the mass transfer of the species enhances within the ECS. High velocity fluid motion is experienced within the ECS for higher Grashof numbers resulting in thinner mass and thermal boundary layers as shown in Fig. 9. This situation should be monitored carefully by an imaging system to categorize and correlate it against the brain disorders.

The influence of varying Lewis number ($Le = \alpha/D$) on the concentration maps, streamlines, and isotherms is illustrated in Fig. 10. Lewis number is defined as the ratio of thermal diffusivity to solutal diffusivity. For a Lewis number of one, heat and solute diffuse in equal extent,

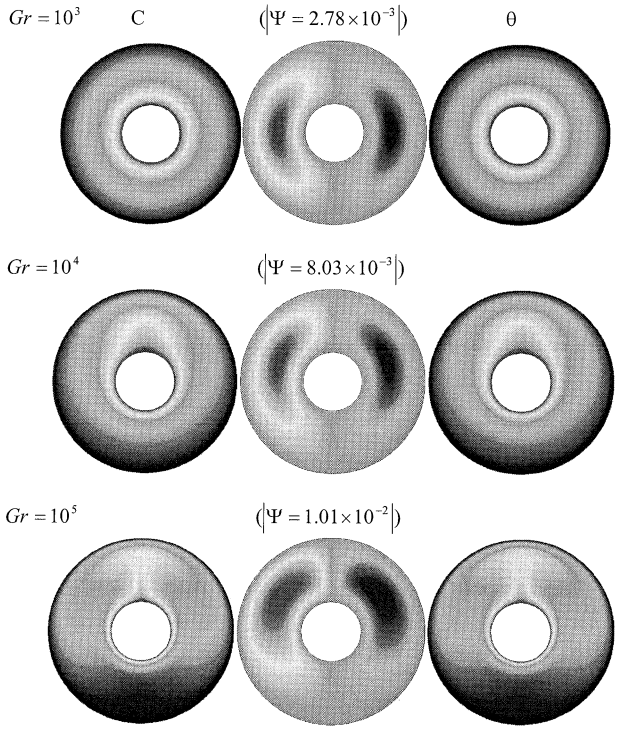

Fig. 8. Effect of the Grashof number on the isoconcentrations, streamlines and isotherms ($Da = 10^{-3}$, $Le = 1.0$, $N = 1.0$, $\varepsilon = 0.2$).

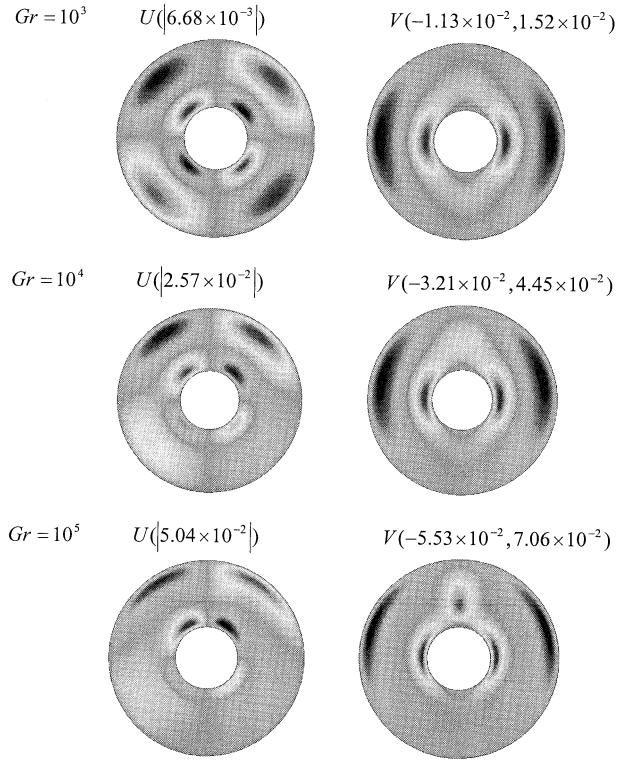

Fig. 9. Effect of Grashof number on the velocity components ($Da = 10^{-3,}$ $Le = 1.0$, $N = 1.0$, $\varepsilon = 0.2$).

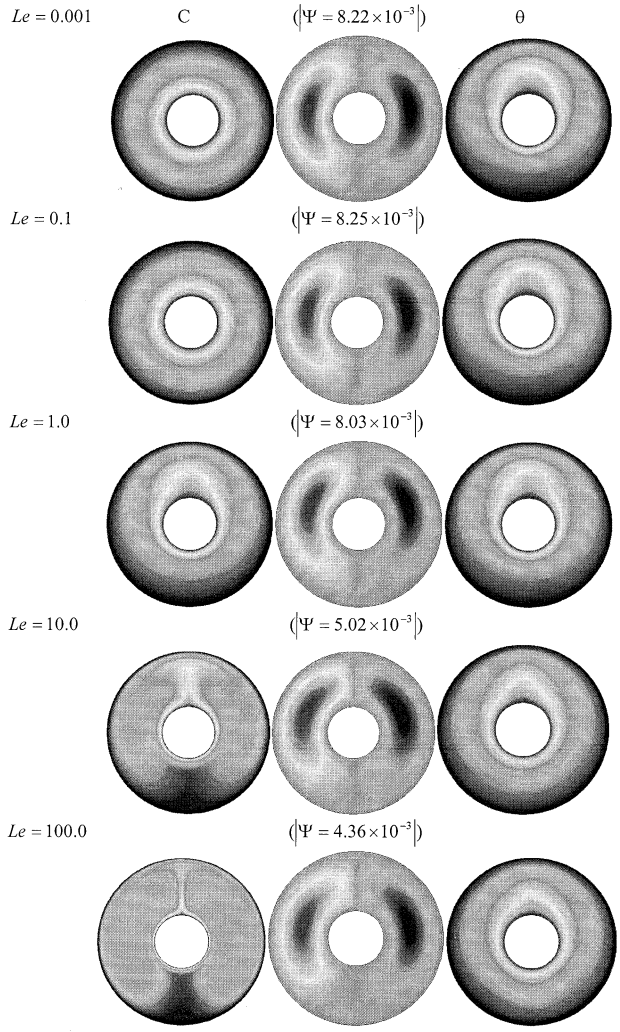

Fig. 10. Effect of Lewis number on the isoconcentrations, streamlines and isotherms ($Da = 10^{-3}$, $Gr = 10^4$, $N = 1.0$, $\beta = 0.2$).

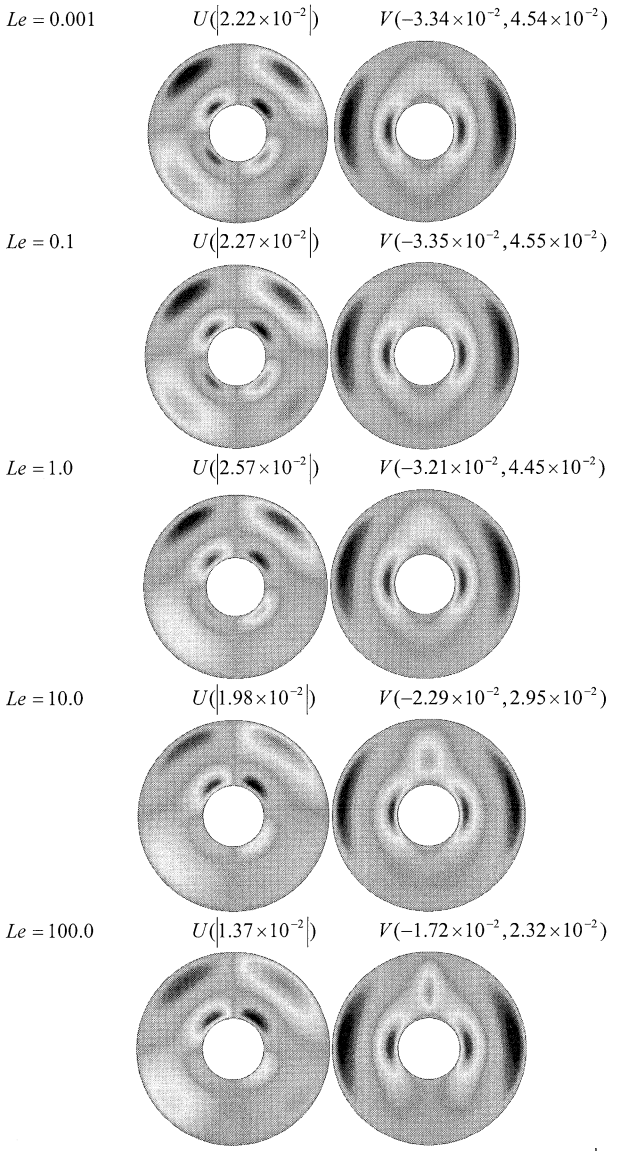

Fig. 11. Effect of Lewis number on the velocity components ($Da = 10^{-3}$, $Gr = 10^4$, $N = 1.0$, $\varepsilon = 0.2$).

which leads to exactly identical heat and mass transfer fields as shown in Fig. 10. For small value of the Lewis number, the water transport in the extracellular space occurs mainly by diffusion. As the Lewis number increases, the solutal boundary layer thickness decreases resulting in a mass transfer enhancement within the brain. The reduction in the diffusion coefficient is due to the effect of the tortuosity. Tortuosity is a measure of the hindrance imposed by cellular structures of the brain and the connectivity of the spaces on the fluid as it moves randomly in the void spaces. As the turtousity of the extracellular space increases, the apparent diffusion coefficient of water decreases and accordingly affects the water movement within the ECS. The effect of Lewis number on the fluid circulation and the flow velocity within the ECS is clearly shown in Figs. 10 and 11.

The effect of varying the concentration between the inner and outer surfaces of the cell on the isoconcentrations, streamlines, and isotherms as well as the velocity components is shown in Figs. 12 through 15. The variation in the concentration is represented by a non-dimensional parameter N that characterizes the ratio between solutal and thermal buoyancy forces. For negative values of the buoyancy ratio ($N < 0$), depending on the value of the concentration expansion coefficient β_c the solutal buoyancy force reverses the thermal buoyancy force as shown in Fig. 12. For larger negative values of the buoyancy ratio ($N \leq -5$) higher heat and mass transfer gradients exist due to dominant mass species buoyancy force. An interesting situation is observed in Fig. 12, which is related to the buoyancy ratio $N = -1$. This scenario illustrates that both solutal and thermal buoyancy forces cancel each other resulting in primarily heat and

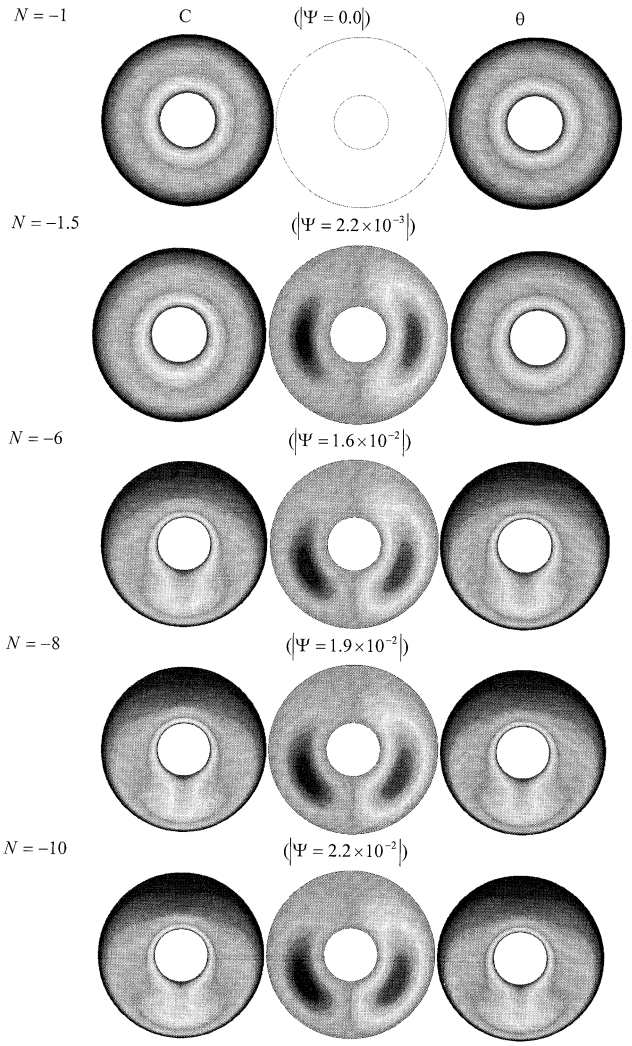

Fig. 12. Effect of negative buoyancy ratio on the isoconcentrations, streamlines, and isotherms ($Da = 10^{-3}$, $Gr = 10^4$, $Le = 1.0$, $\varepsilon = 0.2$).

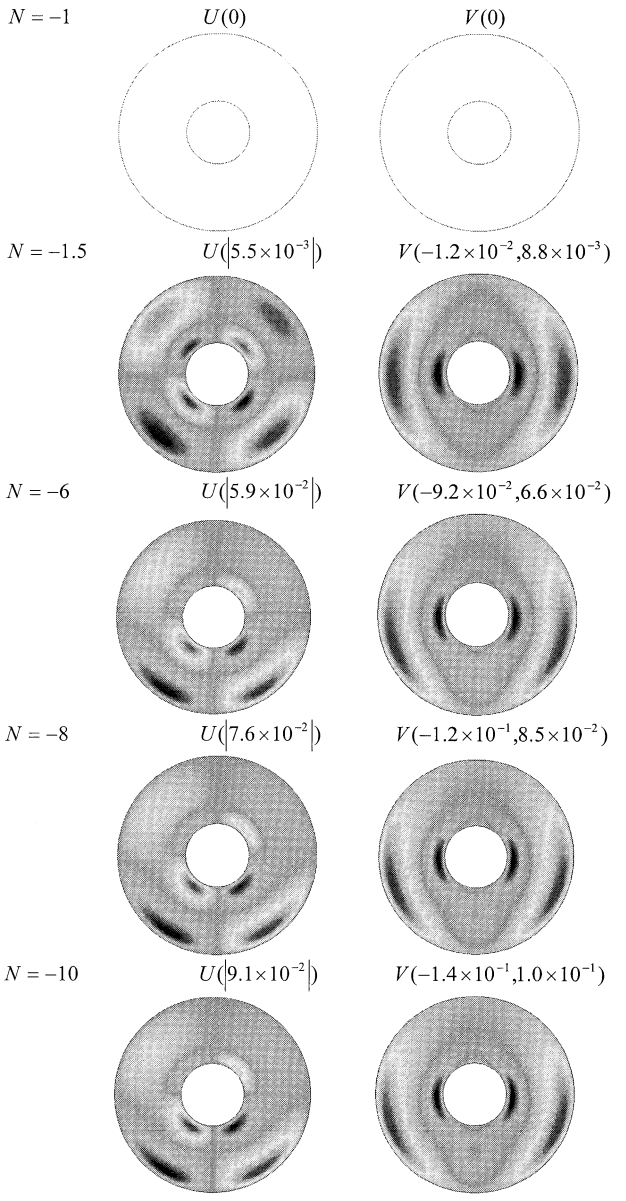

Fig. 13. Effect of negative buoyancy ratio on the velocity components ($Da = 10^{-3}$, $Gr = 10^4$, $Le = 1.0$, $\varepsilon = 0.2$).

mass transfer diffusion processes as indicated by a motionless fluid within the brain. This scenario is clearly shown in Fig. 14, which represents the velocity components for various buoyancy ratios. For buoyancy ratio $N = -1$, the fluid within the brain is essentially stagnant.

Figs. 14 and 15 show the effect of positive buoyancy ratio on the isoconcentrations, streamlines, and isotherms as well as the velocity components within the ECS. When N is sufficiently small, the buoyancy forces that drive the fluid motion is mainly due to the temperature gradients. As such, the thermal buoyancy force drives the fluid motion and the distribution of the constituent does not influence the flow pattern and heat transfer rate in the brain. As the buoyancy ratio increases, the solutal contribution is no longer negligible and cooperates with the thermal contribution to increase the convective amplitude. As a result, diffusion process is overwhelmed by the combined effects of the solutal and thermal buoyancy forces. Furthermore, as $N \to \infty$, the solutal force prevails and the extracellular space becomes solute regime as depicted in Fig. 14. It is evident from Fig. 15 that as the buoyancy ratio increases the fluid velocity intensifies within the brain.

5. Conclusions

Diffusion-weighted magnetic resonance imaging offers an effective technique in the assessment of brain stroke.

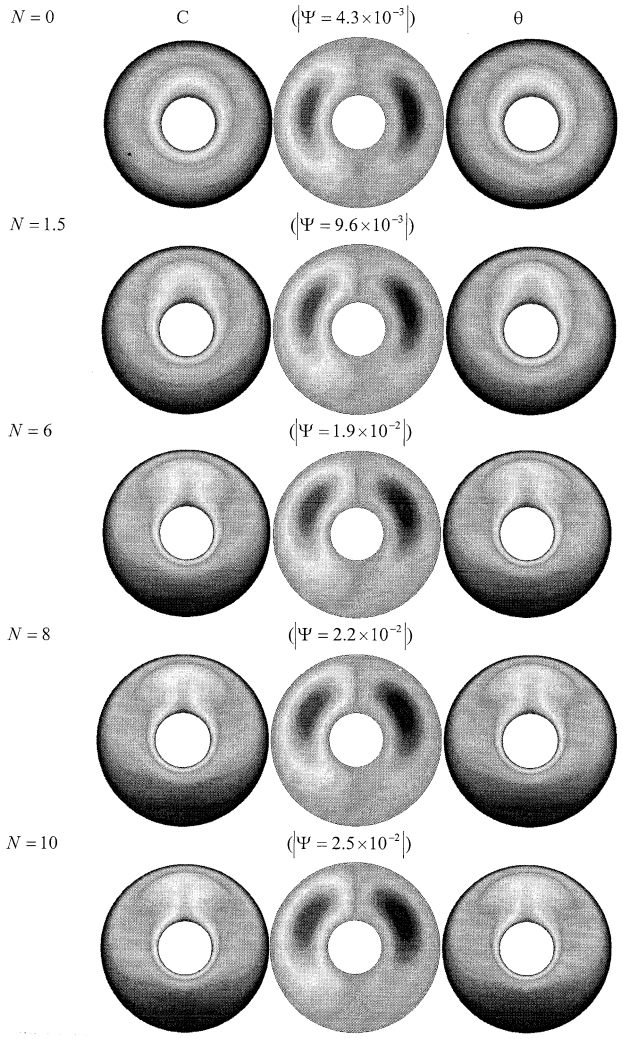

Fig. 14. Effect of positive buoyancy ratio on the isoconcentrations, streamlines, and isotherms ($Da = 10^{-3}$, $Gr = 10^4$, $Le = 1.0$, $\varepsilon = 0.2$).

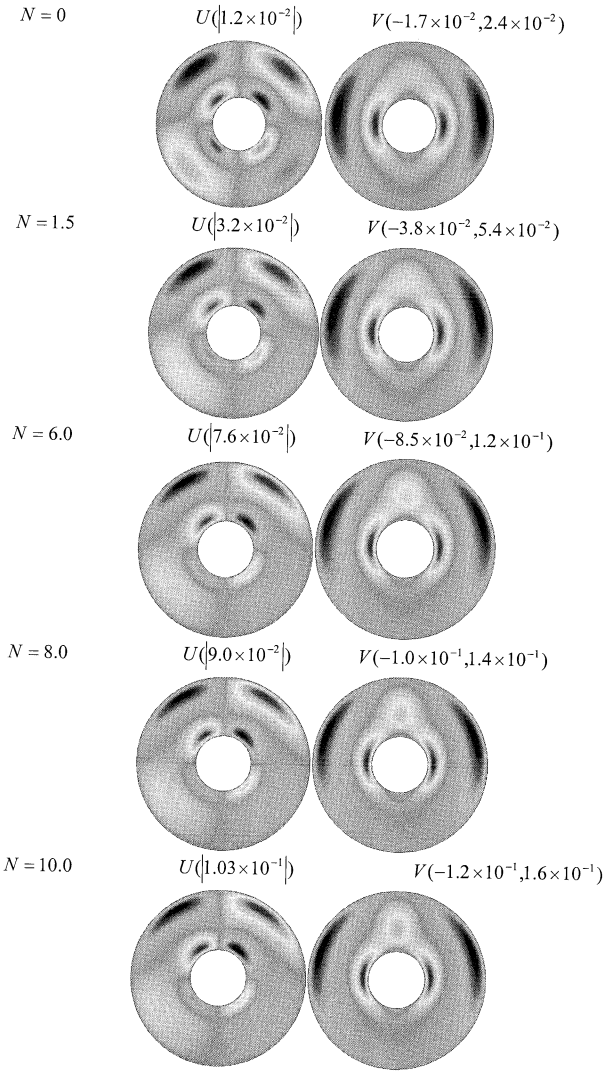

Fig. 15. Effect of positive buoyancy ratio on the velocity components ($Da = 10^{-3}$, $Gr = 10^4$, $Le = 1.0$, $\varepsilon = 0.2$).

Mapping of the calculated apparent diffusion coefficient can be useful in improving the detection and characterization of central nervous system injury. Water diffusion process within the extracellular space is simulated in this work for various pertinent parameters such as porosity, turtousity, Darcy number, diffusion coefficient, Grashof number and the buoyancy ratio. Concentration maps for various clinical conditions are developed and analyzed in the present investigation. The present results show that the diffusion process is dominant within the extracellular space for significantly small Darcy numbers (small permeability). Furthermore, the results show that the diffusion process is overwhelmed by the effect of the solutal buoyancy force for high Lewis number (higher solute transport relative to the thermal diffusion). The present investigation helps in understanding the challenges in applying such a tool to pathology, in particular stroke.

References

[1] Warach S, Dashe JF, Edelman RR. Clinical outcome in ischemic stroke predicted by early diffusion-weighted and perfusion magnetic resonance imaging—a preliminary analysis. J Cereb Blood Flow Metab 1996;16:53–9.

[2] Bose B, Jones SC, Lorig R, Friel HT, Weinstein M, Little JR. Evolving focal cerebral ischemia in cats: Spatial correlation of nuclear magnetic resonance imaging, cerebral blood flow, tetrazolium staining, and histopathology. Stroke 1988;19:28–37.

[3] Norris DG, Niendor T, Leibfritz D. A theory of diffusion contrast in healthy and infracted tissue. In: Proc. of SMRM, 12th Annual Meeting. New York: SMRM, 1993:579.

[4] Latour LL, Svoboda K, Mitra P, Sotak CH. Time dependent diffusion of water in a biological model system. Proc Natl Acad Sci USA 1991;91:1229–33.

[5] Moseley ME, Cohen Y, Mintorovitch J, Chileuitt L, Shimizu H, Kucharczyk J, Wendland MF, Weinstein PR. Early detection of cerebral ischemia in cats: comparison of diffusion and T2-weighted MRI and spectroscopy. Magn Reson Med 1990;16:330–346.

[6] Mintorovitch J, Moseley ME, Chileuitt L, Shimizu H, Cohen Y, Weinstein PR. Comparison of diffusion and T_2-weighted MRI for the early detection of cerebral ischemia and reperfusion in rats. Magn Reson Med 1991;18:39–50.
[7] Benveniste H, Hedlund LW, Johnson GA. Mechanism of detection of acute cerebral ischemia in rats by diffusion weighted magnetic resonance microscopy. Stroke 1992;23:746–754.
[8] Helpern JA, Ordidge RJ, Knight RA. The effect of cell membrane water permeability on the apparent diffusion coefficient of water. In: Proc of SMRM, 11th Annual Meeting, Berlin: SMRM 1992:1201.
[9] Moseley ME, Cohen Y, Kucharczyk J. Diffusion-weighted MR imaging of anisotropic water diffusion in cat central nervous system. Radiology 1990;176:439–45.
[10] Back T, Hoehn-Berlage M, Kohno K, Hossmann KA. Diffusion nuclear magnetic resonance imaging in experimental stroke. Correlation with cerebral metabolites. Stroke 1994;25:494–500.
[11] Prokopova-Kubinova S, Vargova L, Tao L, Ulbrich K, Subr V, Sykova E, Nicholson C. Poly [N-hydroxypropyl) methacrylamide] polymers diffuse in brain extracellular space with same tortuosity as small molecules. Biophys J 2001;80:542–8.
[12] Nicholson C, Rice ME. Diffusion of ions and transmitters in the brain cell microenvironment. In: Flux K, Agnati LF, editors. Volume Transmission in the Brain, Novel Mechanisms for Neural Transmission. New York: Raven Press, 1991. p. 279–94.
[13] Nicholson C. Brain cell microenvironment as a communication channel. In: Schmidt FO, Worden FG, editors. The Neurosciences Fourth Study Program. Cambridge, MA: MIT Press, 1979. p. 457–76.
[14] Sykova E. Activity-related ionic and volume changes in neuronal microenvironment. In: Flux K, Agnati LF, editors. Volume Transmission in the Brain: Novel Mechanisms for Neural Transmission. New York: Raven Press, 1991. p. 217–336.
[15] Lehmenkuhler A, Sykova E, Svoboda J, Ziles K, Nicholson C. Extracellular space parameters in the rat neocortex and subcortical white matter during postnatal development determined by diffusion analysis. Neuroscience 1993;55:339–51.
[16] Nicholson C, Phillips JM. Ion diffusion modified by tortuosity and volume fraction in the extracellular microenvironment of rat cerebellum. J Physiol 1981;321:225–57.
[17] Dai L, Miura R. A lattice cellular automated model for ion diffusion in the brain-cell microenvironment and determination of tortuosity and volume fraction. SIAM J Appl Math 1999;59:2247–73.
[18] Khanafer K, Vafai K, Kangarlu A. Water diffusion in biomedical systems as related to magnetic resonance imaging. Magn Reason Imaging 2003;21:17–31.
[19] Vafai K. Convective flow and heat transfer in variable-porosity media. J Fluid Mech 1984;147:233–59.
[20] Vafai K. Analysis of the Channeling Effect in Variable Porosity Media. ASME J Energy Resour Technol 1986;108:131–9.
[21] Vafai K, Tien CL. Boundary and inertia effects on flow and heat transfer in porous media. Int J Heat Mass Transfer 1981;24:195–203.
[22] Amiri A, Vafai K. Analysis of dispersion effects and Nonthermal equilibrium, non-Darcian, variable porosity, incompressible flow through porous media. Int J Heat Mass Transfer 1994;37:939–54.
[23] Amiri A, Vafai K, Kuzay TM. Effects of boundary conditions on non Darcian heat transfer through porous media and experimental comparisons. Numer Heat Transfer Part A 1995;27:651–64.
[24] Taylor C, Hood P. A numerical solution of the Navier-Stokes equations using finite-element technique. Comput Fluids 1973;1: 73–89.
[25] Gresho PM, Lee RL, Sani RL. On the time-dependent solution of the incompressible Navier-Stokes equations in two and three dimensions. In Recent Advances in Numerical Methods in Fluids, Pineridge, Swansea, UK, 1980.
[26] FIDAP Theoretical Manual. Fluid Dynamics International. Evanston, ILL, 1990.
[27] Barbosa Mota JP, Saatdjian E. Natural convection in a porous horizontal cylindrical annulus. ASME Journal of Heat Transfer 1994;116: 621–6.
[28] Weaver JA, Viskanta R. Natural convection in binary gases due to horizontal thermal and solutal gradients. J Heat Transfer 1991;113: 141–7.